WILEY

ENERGY STORAGE

RESEARCH ARTICLE

Thermal Performance and Shape Stability Evaluation of Boron Nitride and Expanded Graphite Synergy in Beeswax-Based Composite Phase Change Material

Anas Islam[1] | A. K. Pandey[2] | Kosheela Devi Poo Palam[3] | Yasir Ali Bhutto[1] | R. Saidur[1,4]

[1]Research Centre for Nanomaterials and Energy Technology (RCNMET), Faculty of Engineering and Technology, Sunway University, Petaling Jaya, Selengor, Malaysia | [2]Mechanical and Aerospace Engineering Department, College of Engineering, United Arab Emirates University, Al Ain, United Arab Emirates | [3]Advanced Oleochemical Technology Division, Malaysian Palm Oil Board, Kajang, Selangor, Malaysia | [4]School of Engineering, Lancaster University, Lancaster, UK

Correspondence: A. K. Pandey (adarsh.889@gmail.com; adarshp@uaeu.ac.ae)

Received: 10 February 2025 | **Revised:** 23 May 2025 | **Accepted:** 12 August 2025

Funding: The authors received no specific funding for this work.

Keywords: bio-based PCM | energy storage | hybrid additives | shape-stabilized composite | thermal management

ABSTRACT

Phase change materials (PCMs) are efficient thermal energy storage materials due to their high energy density and ability to maintain a constant temperature during phase transitions. Nonetheless, the low thermal conductivity and liquid phase leakage of PCMs constrain their efficient heat transfer and widespread adoption. The development of leakage-free composite PCMs with high thermal conductivity remained a challenge. This work presents the first synergistic enhancement of thermal conductivity and shape stability of beeswax PCM with a dual-scale filler system of h-BN nanoparticles and EG microparticles that has not been reported previously in the literature. The composite containing 3 wt.% of h-BN with 10 wt.% of EG exhibited no leakage at 80°C, with a 312% enhancement in thermal conductivity and a 68.5% decrease in light transmittance. Only a minor reduction of ~12% in latent heat was noted in comparison to the base PCM. Further, the composite exhibited comparable performance after 300 thermal cycles.

1 | Introduction

Significant progress and advancement in industries and technology have been incredibly effective due to a consistent supply of electric power. The extensive use of conventional energy for power production has resulted in numerous worldwide ecological and socio-economic issues. Approximately 20%–30% of the total consumed industrial energy sources are rendered as waste thermal energy and stay untapped. Approximately 65% of the waste heat energy is released into the environment at a temperature of 100°C [1]. The substantial volume of low-grade waste heat is not presently recoverable via economically feasible methods, unlike medium- or high-grade waste heat, which is efficiently used for power generation. Thermoelectric generators may provide a solution for recovering low- and medium-grade heat; however, their poor efficiency, often around 2%, has hindered their industrial adoption. A multitude of research studies and analyses demonstrate that the primary approach to tackling the considerable energy demand–supply gap in an environmentally sustainable way is through the improved integration of renewable energy sources into scalable, cost-effective, and sustainable energy storage systems [2]. Relying solely on a single high-performance energy storage unit is insufficient to address the varied energy requirements effectively. Consequently, a wide range of energy storage methods, including mechanical, electrical, chemical, electrochemical, and thermal systems, is currently the focus of extensive research [3]. Thermophysical and thermochemical storage represent the primary categories of thermal storage solutions. The application of thermophysical storage methods utilizing PCMs demonstrates significant

cost-effectiveness and performance, particularly when contrasted with thermoelectric generators [4]. The thermophysical energies are primarily accumulated as sensible heat, characterized by varying temperature within a single phase, and latent heat, which is maintained at a constant temperature across multiple phases [5]. PCMs play a crucial role in thermal energy storage, as their heat transfer mechanisms can be analyzed at the molecular level and effectively applied to practical applications. The energy storage phenomenon in PCMs arises from the van der Waals interactions that occur among the long-chain polymer molecules [6].

PCMs find extensive application across a multitude of fields, encompassing building and construction for thermal insulation [7], cooling of electronics [8], thermal energy storage in solar power systems [9], regulation of temperature in drug delivery [10], management of thermal conditions in automotive contexts [11], advancements in textile and wearable technology [12], as well as recovery of industrial waste heat [13]. In various applications, the PCMs are engineered to function at specific transition temperatures while exhibiting elevated energy storage densities. Various solid–liquid phase transition-based organic PCMs, including sugar alcohols, fatty acids, and polyethylene glycol, have been extensively studied for thermal energy storage due to their diverse thermal properties [14].

Among all options, paraffin wax stands out as the most dependable phase change material. Its non-toxic characteristics, substantial latent heat, absence of supercooling effects, non-corrosive properties, functionality across various phase transition temperatures, and capability for prolonged use without degradation contribute to its reliability [15]. Nonetheless, paraffin wax PCMs present the most significant financial investment, exert considerable environmental impact, and their manufacturing processes are intertwined with social risks pertaining to safety and health concerns. Conversely, materials derived from biological sources, specifically plant-based options, present a cost-effective solution, ensure safety, open up novel market avenues for agricultural products, and exhibit minimal ecological impact [16]. Appropriately, the carbon footprint of commercial PCMs from raw material extraction to final disposal is also an issue. The environmental impact of producing and using such PCMs may cancel the intended energy savings and carbon reduction benefits [17]. This calls for much more sustainable alternatives, including bio-based and biodegradable PCMs, in addition to improved manufacturing processes and solid waste management methods. Bio-based phase change materials (BPCMs) such as beeswax, palm oil, and coconut oil have several advantages over traditional commercial PCMs [18] which are renewable resources, biodegradability, along with minimal environmental impact. Made from sustainable and natural sources, they reduce the usage of non-renewable resources like petroleum and help the environment to be more resilient [19]. BPCMs are also non-toxic and biodegradable, lessening the level of pollution entering the environment and the health risks related to their creation, use, and disposal [20]. They also often have competitive thermal properties and are therefore suitable for diverse applications in energy storage and thermal management [21]. BPCMs represent a viable option that is in line with the global trend towards greener and more environmentally friendly technology [18]. Among the various bio-based PCMs explored in recent literature, namely fatty acids, plant oils, and bio-derived polyethylene glycols, beeswax is a promising candidate. One of the main benefits of beeswax is the less processing needed. Usually free of chemical synthesis, purification, or hydrogenation, it may be filtered and melted with minimum energy input [22]. By means of intensive extraction, distillation, or transesterification techniques, most plant-derived PCMs, on the other hand, demand energy consumption and probable solvent usage, thereby increasing the environmental effect. Biobased PCMs come in the form of fatty acids, which are often obtained from natural resources including biomass and vegetable oils. BPCMs are characterized by their cheap cost and non-toxic qualities, in addition to their favorable thermal properties as compared to paraffins. However, presently, they are produced from animal tallow or edible crops, which raises issues about the ecology and the safety of food supplies that are available. To soil and marine habitats, beeswax is harmless and biodegradable [23]. Degraded, it breaks down into its original components without producing harmful leftovers. Its end-of-life effect is negligible when compared to certain synthetic PCMs or partly bio-derived formulations including additives, cross-linkers, or encapsulants resistant to breakdown. Beeswax is a product of honeybees (*Apis mellifera*) and it is cultivated sustainably as a material waste. Unlike some bio-based PCMs from large-scale agricultural crops (e.g., palm or soybean oil) beeswax does not compete with food supply or require intensive monoculture farming. From a materials science standpoint, beeswax melts at around 60°C–65°C, so it is appropriate for medium-temperature thermal storage uses such as electronics cooling or construction materials in warm areas. Furthermore, compatible with supporting matrices and nanoparticles, it qualifies for composite PCM systems.

However, all PCMs, commercial as well as BPCMs, show poor thermal conductivity and liquid phase leakage, which seriously hamper their practical implementation despite the numerous advantages they provide. Inadequate thermal conductivity is a significant challenge in applications requiring a quick temperature response [24]. Additionally, since PCMs migrate from solid to liquid during the phase change process, they may leak, leading to material loss as well as compromising the structural integrity of the system and maintenance concerns. These challenges require advanced strategies such as thermal conductivity enhancers or PCMs encapsulated in leak-proof matrices to improve PCMs performance and reliability in real-world applications. Therefore, to develop leakage-proof composite, Zhang et al. [25] created a PEG/carbon aerogel composite using sweet potato as a carbon source from biomass. The composite was synthesized through the vacuum impregnation technique, resulting in excellent form stability, offering a viable solution for efficient thermal energy storage. However, a significant decrease of 29% in latent heat was noted, dropping from 210.3 to 148.8 J/g. In another work, Liu et al. [26] developed a shape-stable PCM composite with improved thermal conductivity and flame-retardant properties to improve thermal safety management of batteries. The incorporation of a porous network structure of expanded graphite (EG) as a shaping support significantly improved the thermal conductivity of PCM from 0.24 to 0.82 W/m K. Furthermore, the incorporation of a silica-based flame retardant that is both environmentally safe and non-toxic (SiO_2 sol) enhanced the flame-retardant characteristics of the material. In another study, Arman et al. [27] developed a PCM composite

TABLE 1 | Key findings from earlier studies on the shape stabilization of PCMs.

References	PCM	Additive	K (W/m K) enahcement (%)	(ΔH_m) reduction (%)
[28]	PEG	SBS+EPDM+AIN	157	40%
[29]	Dodecyl alcohol	Natural zeolite	−44%	55.4%
[30]	Polyethylene glycol	Chemically crosslinked sponge	−29%	7.4%
[31]	Paraffin wax (PW)	Polyethylene/carbon nanotubes	176%	42.02%
[32]		Nickel foam	200%	26.82%
[33]	PW	Graphite	314%	19.18%
This work	Bio-based Beeswax	h-BN/EG	312%	12%

derived from industrial tea waste and investigated its thermophysical performance. The study highlighted that the PCMs, a composite comprising 70% PCM and 30% additive, exhibited excellent thermal resilience. However, a big decline in latent heat from 163 to 55.75 J/g was observed with a minor improvement in thermal conductivity by 27% compared to the base PCM. Table 1 showcases several prior studies conducted by researchers focusing on the shape stabilization of base PCM while improving their thermophysical properties:

It is clear from Table 1 that efforts to improve thermal conductivity led to a significant decline in latent heat, which hampers the energy storage capacity of PCMs. The endeavors to develop leakage free composite PCMs which involved high weight percentages of additives lead to a notable reduction in latent heat capacity. Consequently, attaining high thermal conductivity in PCMs with minimal filler content remains a challenge, to ensure their inherent latent heat is not substantially reduced [27]. Furthermore, despite a lot of advancements in PCM technology, there is still considerable potential in bio-based PCMs with enhanced thermal properties. These gaps highlight the need for developing a bio-based PCM composite that integrates eco-friendliness with robust, long-term thermal performance. This study addresses the shortcomings identified in previous research by using a novel combination of bio-based beeswax PCM, with the synergistic effects of h-BN and EG. The integration of 3% h-BN in conjunction with 10% EG into beeswax has resulted in 312% increase in thermal conductivity while preserving 88% of latent heat. The integration of h-BN and EG improves the structural integrity of PCM and enhances its thermophysical properties. The results highlight the promising prospects of integrating h-BN and EG into advanced PCM composite for diverse thermal energy storage applications.

2 | Materials and Methods

The base PCM beeswax was procured from a local Malaysian supplier, exhibiting a purity of 99%, a latent heat capacity of 121 J/g, and a melting point ranging from 65°C to 67°C. The graphite flake (GF) provided by Sigma Aldrich (China) exhibitedan expansion volume of 220 mL/g. While the hexagonal boron nitride (h-BN) was procured from LFC Canada. The thermal and physical properties of PCM and additive are detailed in Table 2. A rigorous heating operation at 1000°C in a tube furnace was conducted to transform graphite flakes into EG.

TABLE 2 | Key thermal and material properties of PCM and additives.

Properties	PCM-BW	h-BN	GF
Thermal conductivity (W/m K)	0.25	~450	—
Melting temperature (°C)	65	3000	3655
Color	Yellow	White	Silver
Melting Enthalpy (J/g)	121	—	—
Size	—	70 nm	< 50 μm
Purity	≥ 99%	> 99%	> 99%
Density (g/cm^3)	0.970	2.5	100 [34]

2.1 | Development of Expanded Graphite

The flake graphite underwent an intense heating procedure that transformed it into heated EG, leading to the creation of a structure with pores. The EG was subjected to thermal expansion at 1000°C in a hot tube furnace [35]. To ensure that the graphite flakes developed to their full potential, they were kept in the furnace for 30 min. After being subjected to heat processing, the graphite flakes transformed into a worm-like structure and were referred to as EG [36]. The high temperature of the furnace results in the swift enlargement of the graphite flakes, producing porous EG. The obtained EG structure is ideal for encapsulating liquid PCM while enhancing the composite thermal conductivity [37]. Figure 1 shows the conversion of natural graphite flakes into EG using the thermal expansion process.

2.2 | Composite Phase Change Material Preparation

The composite preparation starts with the incorporation of h-BN into the base PCM by ultrasonication to produce nano-enhanced PCM (NePCM). For this, the BW PCM was heated to a molten state in a beaker; then h-BN nanoparticles were added. Ultrasonication was performed at a frequency of 20 kHz, while maintaining the temperature at 80°C for 20 min to achieve consistent mixing [38]. h-BN was included in several weight percentages into the PCM, namely 1%, 3%, and 5%; after which the thermal conductivity of

each NePCM sample was assessed. The maximum thermal conductivity was achieved at 3% h-BN; after which it begins to decline. Detailed discussion is provided in the subsequent Section 3.4. Consequently, to prepare the nano-enhanced shape-stabilized PCM composite with EG, a constant proportion of 3 wt.% h-BN nanoparticles was fixed based on its ability to maximize thermal conductivity. Thereafter, EG was added to the prepared NePCM mixture at varying concentrations of 5 wt.% ($CPCM_5$), 7.5 wt.% ($CPCM_{7.5}$), and 10 wt.% ($CPCM_{10}$) using the vacuum impregnation process. Figure 2 illustrates the comprehensive sequential process for the preparation of the shape-stabilized composite PCM. The experimental process commenced by heating a predetermined quantity of the NePCM (BW/h-BN) mixture to 70°C until it was fully liquefied. The treated EG samples were subsequently infused with the melted NePCM. To enhance the absorption process, the mixture was subjected to a vacuum oven at 80°C for 24 h, at a continuous 100 MPa vacuum pressure enabling capillary forces and surface tension to effectively aid complete integration of BW/h-BN into the EG structure [37]. Magnetic stirring was conducted intermittently for 5 min at 8-h intervals to ensure uniform adsorption. Upon achieving the desired absorption, the shape-stabilized composite (CPCM) in its final powdery form was pulverized into tablets for subsequent evaluation of thermophysical properties.

2.3 | Characterization

The microstructure of PCM and composites was examined with a TESCAN VEGA 3 scanning electron microscope (SEM) integrated with VEGAS software tools. Fourier Transform Infrared (FTIR) spectroscopy was performed utilizing spectrum 2 procured from Perkin Elmer, USA at a wavenumber range from 400 to 4000 cm^{-1} with a resolution accuracy of 0.01 cm^{-1}. The leakage resistance test was evaluated by placing samples on filter paper and exposing them to 80°C (15°C above the PCM's melting point) over the hot plate for 30 min. Optical absorbance and transmittance with a wavelength range from 280 to 1400 nm (UV, visible, and infrared) were assessed on a LAMBDA 750 UV Vis spectrophotometer (Perkin Elmer, USA). The thermal conductivity of the composite samples was determined using Transient Hot Bridge (THB-500, Germany) with a broad operating temperature range up to 700°C. The Differential Scanning Calorimeter (DSC 3500

FIGURE 1 | Production of thermally processed expanded graphite.

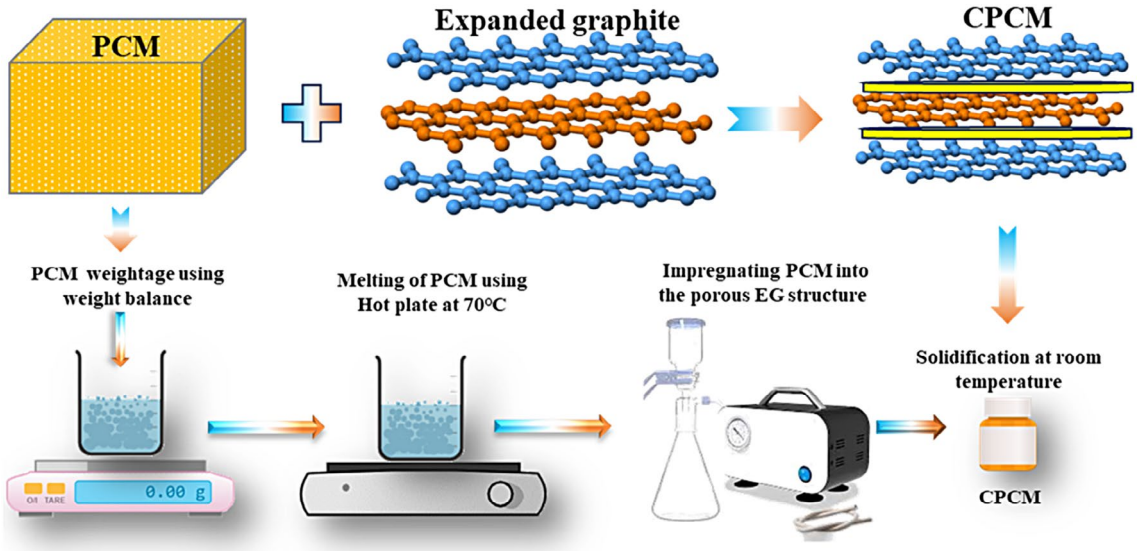

FIGURE 2 | Schematic for preparation of shape-stabilized CPCM.

Sirius) made by NETZSCH, Japan was used to assess the latent heat and melting point of samples. Finally, the optimal PCM composite ($CPCM_{10}$) was subjected to 300 thermal cycles in a thermal cycler equipped with a custom copper plate at a temperature variation rate of 15°C per minute for reliability assessment.

3 | Results and Discussion

3.1 | Morphology Assessment of Base BW and CPCM

Scanning electron microscope (SEM) was utilized to acquire images of high resolution for the analysis of the morphological features of the materials. Figure 3a–e illustrate the SEM images of PCM-BW, h-BN nano-particles, EG, BW/h-BN, and CPCM shape stable composites. Honeybees generate beeswax in a liquid state at ambient temperature. Subsequently, it hardens into scales as soon as it encounters the surroundings [23]. The amorphous and heterogeneous nature of the components constituting beeswax, seen in Figure 3a, exhibits a foggy, colloidal, and pasty appearance. The configuration illustrated represents a unique lattice made up of pure beeswax phase change material, featuring multiple air cavities. As the temperature surpasses the melting point of PCM-BW, the lattice structure begins to melt gradually, leading to a transition in the liquid profile [39]. Furthermore, the layered structure of beeswax reflects its crystalline nature, consisting of a continuous matrix with some air pockets. Thermophysically, this structure influences the melting behavior, since the PCM changes from solid to liquid layer-by-layer when heated [39]. This stratified melting leads to a slow thermal response and may affect the dispersion and integration of additives such as EG and h-BN by directing the molten matrix flow around the filler surfaces and thus influencing thermal transport pathways in the composite. Figure 3b shows the hexagonal layered structure of h-BN, hence revealing its morphology. The structure of the crystal lattice between boron and nitrogen atoms shows this arrangement. Figure 3c illustrates the SEM image of EG; after the process of thermal treatment, the

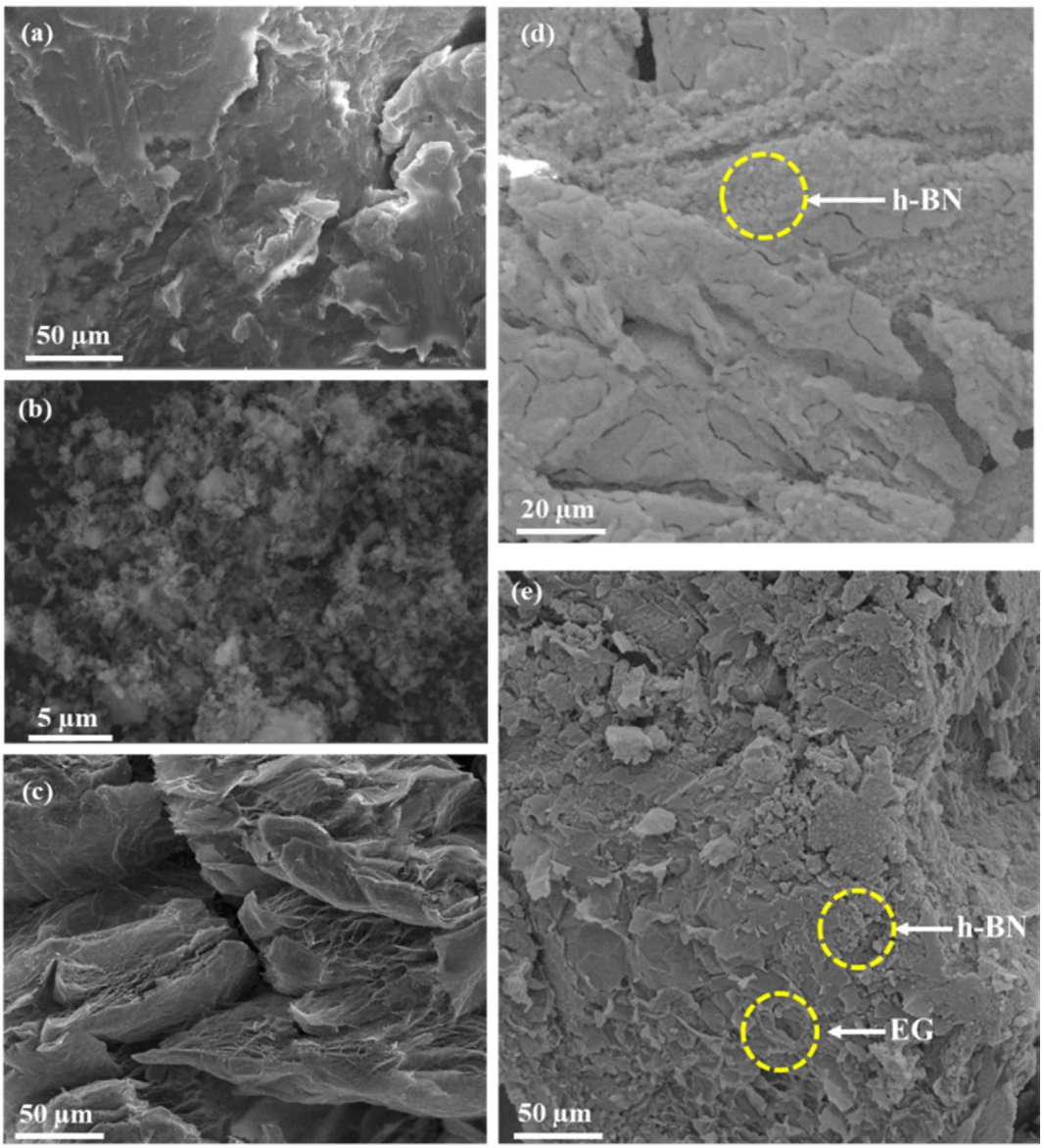

FIGURE 3 | SEM morphology: (a) base BW at 50 µm, (b) h-BN nanoparticle at 5 µm, (c) EG at 50 µm, (d) BW/h-BN NePCM composite at 50 µm, (e) shape stable CPCM composite.

graphite flake is shown to have increased size resulting in a worm-like structure [40]. The microstructure of EG forms both flat and honeycomb-like structures. Honeycomb structures help in the adsorption of PCM served by EG's honeycomb capillarity action, which prevents leakages [37]. The PCM infiltrates the voids within the EG structure, resulting in a composite material where the PCM is effectively incorporated and encapsulated inside the porous scaffold. Figure 3d illustrates the microstructure of BW/h-BN NePCM composite, where the small white dots show the uniformly distributed h-BN particles within the PCM-BW. Additionally, the image shows the transition in the surface morphology from a uniform and refined texture of pure PCM-BW to a coarse and irregular structure. This surface morphological alteration indicates the effective incorporation of h-BN nanoparticles into PCM-BW.

Figure 3e illustrates the SEM image of the developed CPCM composite. The BW/h-BN NePCM composite has been completely absorbed inside the pores of EG due to its capillary action. This configuration prevents the molten beeswax from leaking during phase transitions and facilitates the attainment of enhanced thermal conductivity. Due to the existence of chemical and physical forces, such as hydrogen bonding and van der Waals interactions, the adsorption phenomenon exhibits significant resilience [34]. These forces make it easier for the BW/h-BN NePCM composite to penetrate the porous structure of EG. Therefore, the outcomes demonstrate that EG can perform the role of a covering material, which enables it to provide effective adsorption without leakage.

Additionally, energy-dispersive X-ray spectroscopy (EDS) was used to ascertain the elemental composition of the PCM-BW, h-BN, EG, and CPCM composite. All obtained results are displayed in Figure 4. The EDS analysis findings, as shown in Figure 4a, indicate that the beeswax sample had the highest bulk carbon content with the largest atomic percentage (91.38%), indicating its carbon-rich nature. The EDS analysis of h-BN nanoparticles, as illustrated in Figure 4b, confirms the presence of boron (B) and nitrogen (N) content in their elemental composition [41]. Figure 4c shows the EDS of EG revealed a dominating carbon peak, confirming its high-purity composition. No additional elemental signals are found, which suggests the consistency and homogeneity of the material. As illustrated in Figure 4d, the EDS analysis of the $CPCM_{10}$ composite verifies the presence of element C from PCM-BW and EG, while B and N originated from h-BN. Elemental analysis detected only B, N, and C, with no identifiable contaminants. Attributed to the coating used during sample preparation, a little platinum (Pt) peak was seen. Moreover, elemental mapping shows homogeneous distribution of B, N, and C, thereby showing homogeneous dispersion of BW/h-BN mixture within the porous EG structure.

3.2 | Chemical Composition Analysis of BW and Composite PCMs

The FTIR Analysis or FTIR Spectroscopy is a method of analysis that is used for the purpose of determining the composition of organic and inorganic substances. For analyzing chemical characteristics, the FTIR technique employs infrared light to scan test materials [42]. Figure 5 shows the FTIR spectra of BW and composite PCM at 2921 and 2851 cm^{-1} respectively, which correspond to the CH_2 and CH_3 stretching vibrations. The peak at 1741 cm^{-1} is due to in-plane bending of CH_2 and CH_3 bonds, and the 1465 cm^{-1} peak to CH_2 in-plane vibrations. Furthermore, the peak at 1166 cm^{-1} represents the in-plane bending of several bonds, and the peak at 720 cm^{-1} represents the C-H rocking mode characteristic of the methyl groups in long-chain alkanes (usually in the 725–720 cm^{-1} range). In the BW/EG PCM composite spectrum, peaks are observed at 2921, 720, 1166, 1741, and 2851 cm^{-1}, indicating retention of beeswax characteristics. No other significant peaks attributed to EG and h-BN particles were detected. These results indicate that beeswax, h-BN, and EG-based composite PCM maintains physical interaction without any chemical reaction during the composite preparation process.

The FTIR spectra show no new chemical bonds are created—suggesting physical rather than chemical interaction—this kind of interaction remains vital for structural integrity and heat transport because of strong interfacial contact between the components. This chemical stability is crucial as it confirms that no degradation, side reactions, or formation of new functional groups occurred during repeated melting and solidification processes. This kind of stability has a direct influence on the thermal performance of the composite material because it guarantees reliable phase-change behavior and the retention of latent heat over the course of time. The composite, in contrast to other PCM composites, which are susceptible to oxidative degradation or chemical interaction with supporting materials, was able to sustain its integrity, as shown by the fact that its FTIR spectra were conserved. This indicates that the thermal dependability of the system is superior to that of PCM systems that are more reactive or less stable, as documented in the literature. For example, research reveals that the chemical stability of rubber elastomers such as NR, SBR, NBR, and EPDM (raw, gum, reinforced, and their polyblends NR/NBR and NR/EPDM) has a significant impact on the thermal and mechanical performance of the material. The FTIR spectrum observations showed that NR has a high molecular compatibility with both NBR and EPDM. This indicates that the chemical structures of NR are stable and have a limited number of functional groups that are susceptible to degradation. Measured tensile strength data by ASTM techniques suggest that the blends achieve increased elasticity and tensile performance via enhanced interfacial bonding and uniform dispersion of elastomer chains [43]. This chemical stability is connected to mechanical behavior since the measurement of tensile strength indicates that the blends accomplish this. Comparing this phenomenon to PCM composites, where the chemical compatibility between the PCM and the supporting matrix is essential for performance, reveals that it is as crucial.

3.3 | Leakage Test of Developed Composite

PCMs are utilized in various sensitive applications, and leakage testing is a crucial part in guaranteeing their reliability and safety. It is crucial to conduct these tests to assess the integrity of PCM containment devices, like capsules or enclosures, and then to recognize some possible leaks which might influence performance or safety problems. Figure 6 depicts the leakage effectiveness of the developed PCM composites, as opposed to the base PCM-BW. The samples were placed on filter paper and heated on a hot plate at 80°C, approximately 15°C above the melting

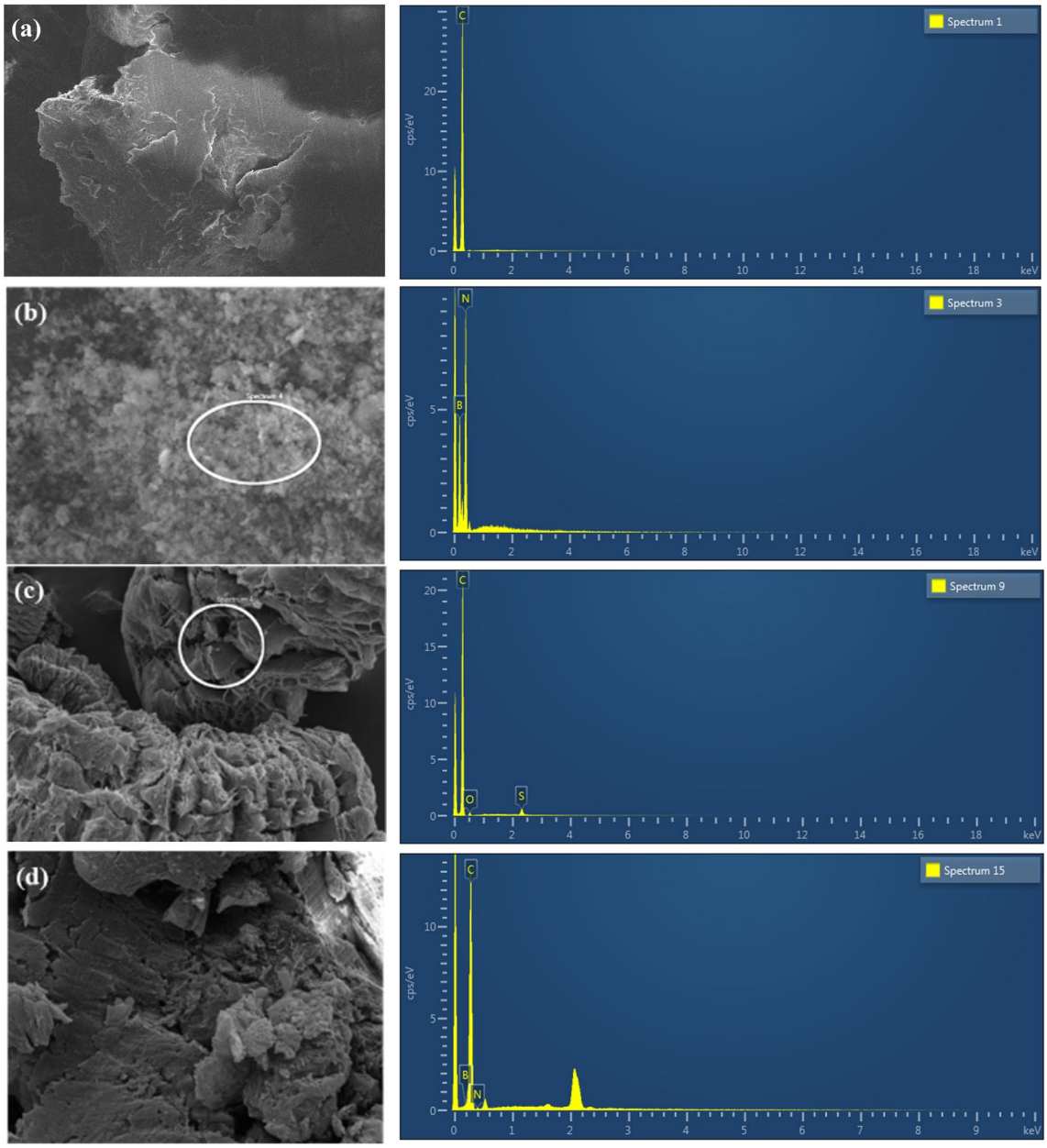

FIGURE 4 | Energy-dispersive X-ray spectroscopy analysis for (a) PCM-BW, (b) h-BN nanoparticles, (c) expanded graphite, (d) developed $CPCM_{10}$ composite.

point of base PCM. Throughout the heating process, the composite $CPCM_{10}$ material maintained its structural integrity and demonstrated exceptional thermal stability. Nevertheless, the additional two composites, $CPCM_5$ and $CPCM_{7.5}$, showed leakages after 20 min, indicating that lower levels of additives were insufficient to completely stop leakage of PCM. The base PCM BW, on the opposite hand, underwent a complete deformation because of complete leakage after 30 min. Following the leakage test, it was demonstrated that $CPCM_{10}$ composite had a higher degree of form stability as it demonstrated no sign of leakage even after 30 min. Furthermore, it managed to keep its original shape, demonstrating the synergy of the additives (h-BN/EG) scaffold in maintaining structural integrity and preventing leakage during phase transitions. It may be affirmed that weak links, like capillary forces, hydrogen bonds, and surface tension forces, are accountable for the confinement of the PCM [44]. Low wt.% loadings ($CPCM_5$ and $CPCM_{7.5}$) leak due to inadequate EG matrix content compared to PCM. At lower EG levels, the porous structure may not absorb and entirely encapsulate PCM, leaving extra on the composite surface. This PCM is prone to leakage, especially during the phase transition. A similar observation was made during previous experiments where samples with lower EG content showed visible leakage due to unabsorbed PCM accumulating on the surface. However, this excess PCM was removed by surface treatment after the leakage was reduced [45]. However, larger EG content ($CPCM_{10}$) provided enough porous volume to absorb and prevent PCM leakage. PCM is uniformly distributed into the EG structure by vacuum impregnation, preventing voids and gaps. So, $CPCM_5$ and $CPCM_{7.5}$ leak because PCM absorption is low owing to low EG concentration.

For applications such as example battery thermal management, in which PCMs are employed to absorb and dissipate heat, it is essential to ensure their containment to prevent fire risks while preserving the operational efficiency [46, 47]. Determining some leakage in PCM containment systems is made possible using leakage testing methods. This enables timely repairs or maybe replacements being made, which helps to limit hazards and makes sure that the device continues working for a prolonged period. Moreover, extensive leakage testing boosts trust in PCM-based technologies, which motivates their wider adoption across an assortment of sectors.

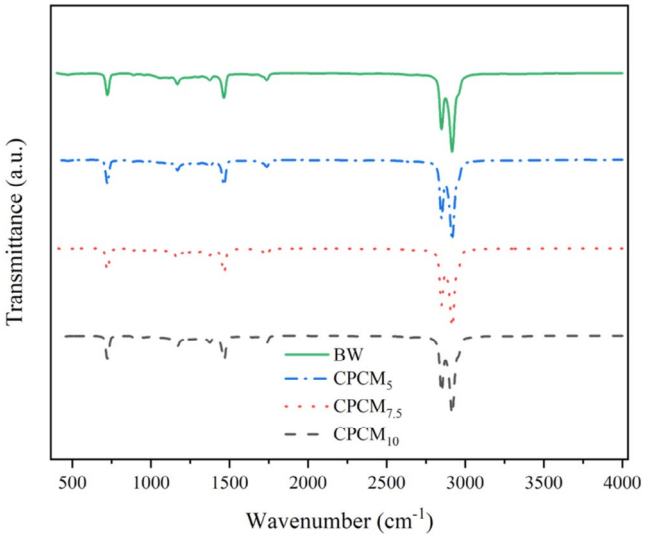

FIGURE 5 | The FTIR spectra of BW PCM and the CPCM.

To assess the composite's long-term resistance to leakage; future studies should conduct prolonged duration tests at higher temperatures (80°C–100°C for 24, 48 and 72 h respectively). The leakage test might also be carried out under controlled humidity (60%–90% RH) and incorporate mechanical stress loads (e.g., 1–10 N of compression) in order to simulate environmental and application-specific conditions. Such improved test settings would make it possible to have a better understanding of the long-term endurance of the composite $CPCM_{10}$, which might be used in applications such as electronic or battery cooling solutions.

3.4 | Heat Transfer Assessment of PCM and Composites

The thermal conductivity of the PCMs plays a major part in heat transfer characteristics. Figure 7 depicts the thermal conductivity values for PCM and composites. The thermal conductivity of the composite samples was determined using Transient Hot Bridge (THB-500, Germany). The samples had a diameter of 40 mm and a thickness of about 5 mm to provide sufficient contact area and uniform heat transfer. Each sample was tested three times at room temperature (25°C ± 1°C). The average value was reported, and the standard deviation for experimental uncertainty was calculated.

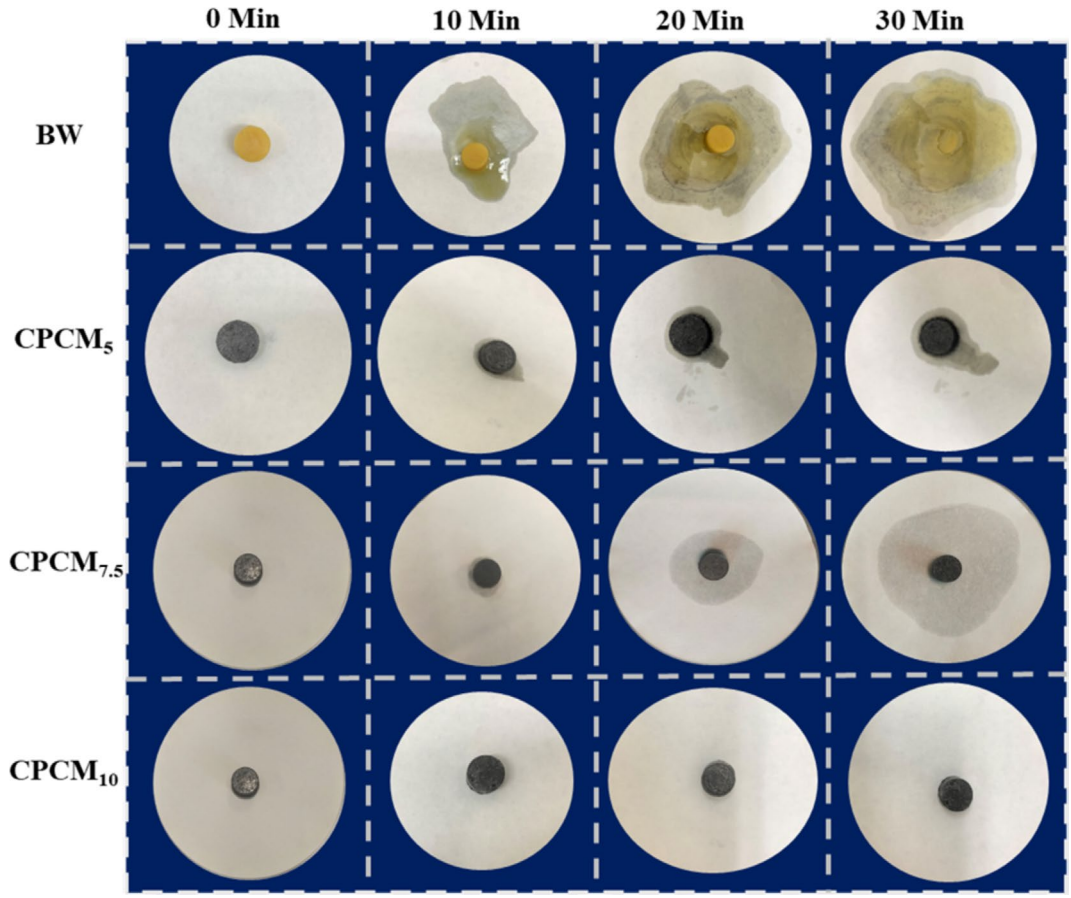

FIGURE 6 | Leakage behavior of PCMs and developed composite tested for 30 min.

The thermal conductivity of base PCM BW was measured at 0.25 W/m K. While the thermal conductivity after the addition of h-BN nanoparticles to BW (BW/h-BN) at weight ratios of 1%, 3%, and 5% was recorded as 0.28, 0.34, and 0.29 W/m K, respectively. This suggests that the NePCM (BW/h-BN) composite achieved a maximum thermal conductivity of 0.34 W/m K at 3% h-BN. On further addition of h-BN particles, the thermal conductivity tends to decrease due to the agglomeration of particles, as shown in Figure 7a.

As a result, this experiment maintained a 3% concentration of h-BN while altering the ratio of EG to determine its minimum quantity required to synthesize the final leakage-free composite. Existing studies [36, 45] verify that thermal conductivity increases linearly with increasing EG concentration. For EG concentrations of 5%, 7.5%, and 10%, the respective thermal conductivity values were 0.65, 0.77, and 1.03 W/m K, respectively, as illustrated in Figure 7b. The interconnected three-dimensional thermal network of EG contributes to the enhanced heat transfer [48]. Furthermore, the porous architecture of EG led to a notable enhancement in the reduction of interfacial thermal resistance, as well as facilitating effective phonon propagation throughout the composite matrix. At minimal EG concentrations, the CPCM reaches an adsorption saturation point where the porous surface of the EG is completely coated with liquid PCMs and convection

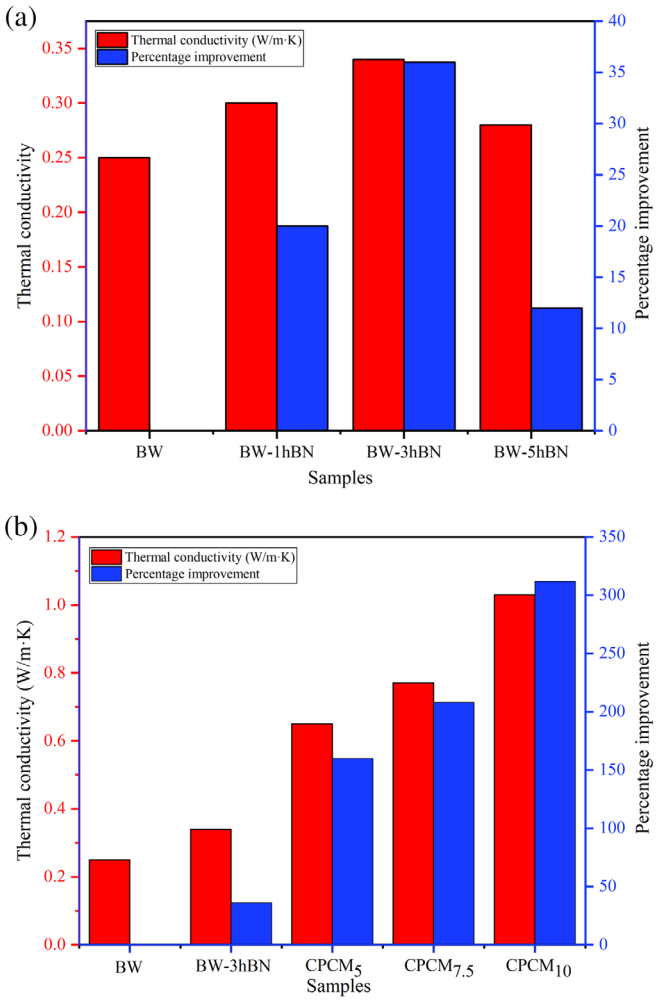

FIGURE 7 | Bar chart illustrating the thermal conductivity of (a) NePCM (h-BN/BW) samples and (b) shape-stabilized samples.

is the dominant heat transfer mode. As the concentration of EG increases, the microporous framework of EG becomes saturated with liquid PCMs to facilitate heat transfer. This process of convection continues until adsorption is no longer taking place, and the primary mode of heat transmission is shifted to conduction [49]. Since $CPCM_{10}$ has better overall performance and does not exhibit any leakage, the 3% h-BN enhanced BW/EG composite containing 10 wt.% of EG is a viable PCM composite.

The Table 3 shows that whilst many paraffin-based systems show significant conductivity gains depending on large loadings of EG, graphene, or metallic fillers, this composite shows a corresponding or better boost at lower filler concentrations. This emphasizes harmonically integrating h-BN nanoparticles with EG microstructures in a bio-based PCM matrix such as beeswax effects.

3.5 | Latent Heat Evaluation

Differential Scanning Calorimetry (DSC) is used to evaluate the melting enthalpy and phase transition temperatures of the base PCM and composites. Figure 8 shows the melting and freezing curve behavior of the PCM and composites. The thermal profiles of the base and composite PCMs show the same heating and cooling characteristics. Notably, the DSC curve for the melting process shows two endothermic peaks. The first, smaller peak signifies a solid–solid phase change, while the bigger peak signifies the solid–liquid phase change. In the base PCM, the primary melting phase transition occurs around 65°C and solidifies at approximately 54.10°C. For the CPCM composites, the phase transition during the heating process falls within a narrow range of 64.52°C to 67.43°C, showcasing the consistent thermal behavior. Furthermore, the cooling cycle phase change temperature lies between 54.52°C and 56.31°C. The latent heat (area under the DSC curve) is a quantitative measure of the energy absorbed or released during phase changes. A latent heat of 121.76 J/g was measured for the base PCM, while the composites $CPCM_5$, $CPCM_{7.5}$ and $CPCM_{10}$ demonstrated latent heats of 115.68 J/g, 112.63 J/g, and 107.15 J/g, respectively. The observed reduction in latent heat with increasing EG content can be explained by the dilution effect of the PCM matrix caused by the non-phase-changing fillers (h-BN/EG). The overall efficiency of the material is significantly improved due to substantial increases in thermal conductivity and leakage; thus, the 12% reduction in latent heat does not impact the overall performance of the PCM. Previous studies related to the development of shape-stable composite PCMs have resulted in a significant reduction in latent heat, sometimes approaching a 50% decrease [28, 29]. Some studies also show a minor decrease in latent heat of 7% but at the cost of compromising the thermal conductivity of around −29% [30]. This study clearly shows the synergistic role of h-BN and EG in preserving the latent heat of the material while enhancing the thermal conductivity. Consequently, the developed composite demonstrates its significance in applications necessitating a rapid heat response over extended periods.

While in long-term thermal buffering systems or other applications requiring fast thermal response and high heat dissipation—such as battery thermal management or building envelope systems subjected to intermittent solar radiation—this

TABLE 3 | Thermal conductivity enhancement levels with various additives and respective base PCMs.

Filler composition	PCM type	Melting temp (°C)	Support matrix	λ (PCM) (W/m K)	λ (composite) (W/m K)	% increase in λ	References
20% Graphene Powder	Paraffin	48.4	None	0.33	0.74	124%	[50]
1% Expanded Graphite	Paraffin	46.4	None	0.20	—	—	[51]
14% EG + 2% Cu	Paraffin	—	—	0.20	1.98	890%	[52]
3.3% EG + 5.6% h-BN	Paraffin	47.3	Styrene Rubber (61%)	0.21	0.95	352%	[53]
5% EG	Paraffin	46.5	SEPS (9.5%)	0.20	2.67	1235%	[54]
15% AlN	Lauric Acid	47.2	Melamine Foam	0.23	0.37	60%	[55]
8% AlN	PEG	46.5	SBS (41.4%) + EPDM (4.6%)	0.28	0.72	157%	[28]

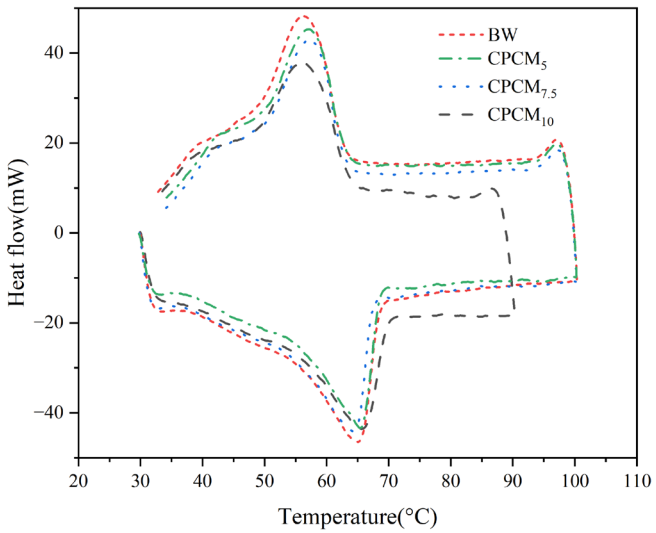

FIGURE 8 | Latent heat evaluation of PCM and composites.

reduction may be a disadvantage in cases where maximum latent heat storage is crucial. A diluting influence is created by the non-phase-change supporting materials (h-BN and EG), which take up space but do not contribute to the storage of latent heat. This impact is responsible for the decline in latent heat, which is the outcome of the diluting impact. This compromise would have significant repercussions in the real world. When it comes to thermal management applications, such as batteries or electronics, where rapid heat dissipation is of utmost importance and the requirement for energy storage is minimal, the enhanced thermal conductivity is more significant than the decrease in latent heat [56]. On the other hand, when it comes to applications that primarily involve energy storage, such as building envelope systems or solar thermal storage, it may be more crucial to maximize latent heat capacity. Additionally, it may be more desirable to have a greater PCM content while also optimizing conductivity [57]. Therefore, the unique application goals should serve as a guiding principle for the selection of composite formulations because of this. For specific use cases, the optimization could be further refined by design strategies such as layering composites with different filler loadings, encapsulation, or using hybrid PCMs with wider melting ranges. The preservation of high latent heat while maintaining directed or localized thermal conductivity may be accomplished by the use of hybrid optimization methodologies, such as layered structures or graded composites, which can be investigated in further study.

3.6 | Thermal Decomposition Assessment

Thermogravimetric analysis (TGA) is a thermal analysis technique that examines changes in the weight loss of materials as a function of temperature [58]. Figure 9 presents the thermal decomposition curves for the base PCM and composite samples that have been impregnated within porous EG. The graph for base PCM BW, $CPCM_5$, $CPCM_{7.5}$, and $CPCM_{10}$ composite samples demonstrates single-step thermal decomposition. The reduction in weight fraction of the sample as temperature rises illustrates this phenomenon. All samples exhibited exceptional thermal stability, maintaining their weight up to 220°C. When this threshold is surpassed, the process of decomposition initiates; it is noted that all PCM composites undergo a weight loss of about 85% within the temperature range of 430°C–450°C. This is since the weight fraction of the PCM decreases as the temperature becomes higher due to evaporation [14]. Following the breakdown of the PCM molecules, the remaining residue consists of h-BN and EG particles, which possess a certain weight fraction. The principal component enhancing the composite's stability under heat is the incorporation of h-BN nanoparticles and porous EG into the base PCM. This addition probably results in the formation of a thermal shield due to capillary effects and van der Waals interactions within the PCM-additive system. These interactions act as an insulating layer, thereby reducing the impact of temperature. The TGA results clearly indicate that the thermal stability of PCM impregnated with EG exhibits a slight enhancement as the concentration of the EG additive is

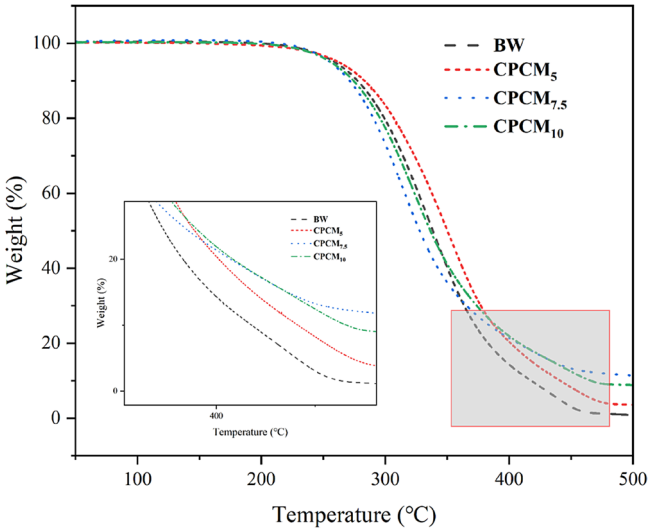

FIGURE 9 | Thermal decomposition curve of base PCM and the composites.

increased. An interesting finding from the results is that the sample with 10% EG ($CPCM_{10}$) shows slightly more weight loss compared to the sample with 7.5% EG ($CPCM_{7.5}$). This may be attributed to the development of micro-composites resulting from the agglomeration of EG microparticles. This little thermal stability loss results from higher loading of h-BN nanoparticles perhaps exceeding the optimum dispersion threshold. At this concentration, partial aggregation of h-BN can occur, generating localized temperature gradients and reduced heat dissipation efficiency during degradation. Such agglomerates may interact with the uniform thermal barrier effect produced by well-dispersed fillers and considerably slow down the deterioration of the composite. This interpretation is corroborated by SEM observations showing small clusters of h-BN in $CPCM_{10}$. Furthermore, the presence of agglomerates can alter the degradation pathways of the composite. Agglomerated particles may act as sites for accelerated degradation, leading to a decrease in the composite's thermal resistance [59]. Further study by particle dispersion analysis or high-resolution TEM would be helpful to quantify this effect more precisely and is recommended for future work. The result of this study is in conformity with the conclusions that were described in past investigations [60, 61]. Moreover, it is encouraging to note that the shape-stabilized PCM composite exhibited a stable character while operating within a temperature spectrum of 200°C, demonstrating optimal thermal conductivity.

3.7 | Investigation of the Optical Behavior of Material

The UV–vis technique was employed to determine the optical absorbance and transmittance of the base PCM and the composite. The optical properties of the organic solid PCM were evaluated by a UV–Vis spectrometer, in which a light beam was passed through the sample. This approach allows accurate analysis of the absorbance and transmittance at different wavelengths to reveal the material's behavior with light. When radiation encounters a material, it may be transmitted, absorbed, or reflected, depending on the specific conditions involved. Solar radiation is typically divided into three distinct categories: (a) the ultraviolet region (280–380 nm), (b) the visible region (380–740 nm), and (c) the near infrared region (740–1400 nm) [45]. PCM can effectively store thermal energy and subsequently release it based on the chosen application. Solar power is the primary source of thermal energy, which emerges in the form of electromagnetic waves. Enhancing the capacity of the composite to absorb solar radiation is crucial. Generally, all organic materials, which serve as base PCMs, exhibit a significant level of transmissibility and are transparent in their natural form [45]. Figure 10a illustrates the absorbance curve showing that the EG-impregnated PCM composites absorb more light than the base PCM. This enhancement in absorbance is due to the synergetic effects of h-BN and EG, which make the composite darker and improve its light-absorbing property. The transmissibility of base PCM, $CPCM_5$, $CPCM_{7.5}$, and $CPCM_{10}$ was found to be 22.75%, 9.5%, 8.4%, and 7.16% respectively, as shown in Figure 10b. The incorporation of 10% EG into the PCM ($CPCM_{10}$) results in a maximum reduction of 68.5% in optical transmissibility. The increase in absorbance resulted in the decrease in transmissibility of composites. Thus, the developed composites have been found to reduce transmissibility while increasing absorbance, which is crucial for applications that require thermal energy from optical rays.

Figure 10 reveals an intriguing phenomenon concerning the existence of a peak at around 1200 nm for BW in both spectra. This peak is much reduced in the majority of composite samples, which is a significant finding. The decrease in the 1200 nm peak may be attributed mostly to the dilution of BW inside the composite material, as well as the reinforcement matrix's enhanced light scattering and absorption. One of the fundamental properties of pure PCM is the strong peak that can be seen in it. Increasing the amount of EG additions, on the other hand, results in a decrease in peak intensity since these additives do not display absorption at various wavelengths. There is no change in the chemical composition of the PCM as a result of this impact, which is entirely physical. There have been prior investigations [34, 62] that have reported similar findings of declining peaks in the absorbance and transmittance curves.

In practice, the amount of solar energy stored in a wall—so called solar energy actually absorbed (SEW)—does not depend only on the material's radiation absorption coefficient. Rather, it is significantly influenced by parameters such as the wall's heat accumulation coefficient, surface heat transfer coefficient, and duration of solar exposure. This implies that materials with better absorption and superior heat retention, such as the developed CPCM, with enhanced absorbance; therefore, it would likely absorb solar energy more effectively [63]. Since the absorbance of the wall-integrated PCM composite is enhanced, more solar energy can be captured and retained within the thermal mass of the building envelope. This allows for more efficient daytime heat storage and delayed nighttime release, improving thermal comfort and reducing auxiliary heating loads. The improved optical behavior of the CPCM confirms its suitability for solar thermal applications as well as passive building design strategies to maximize solar gains in winter and to minimize energy consumption in general. The improved optical behavior thus provides support for better thermal performance as

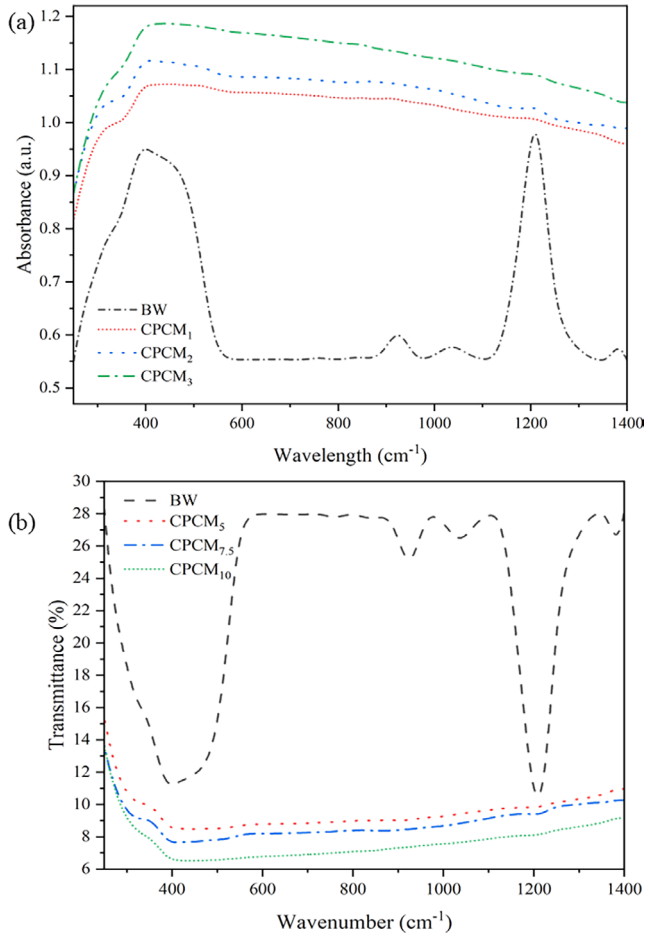

FIGURE 10 | Optical performance analysis of base PCM BW and composites (a) absorbance (b) transmittance of the light rays passed through.

well as energy savings and sustainability in building envelope applications.

3.8 | Thermal Reliability

A thermal cycling test was conducted to look at the thermal stability and reliability of the developed PCM composite over a period. Thermal cycling is used to assess the thermal resilience of PCMs by doing repeated heating and cooling cycles in a controlled time. The experiment used a custom-made thermal cycling system with multiple independent compartments, allowing simultaneous testing of several samples. Composite $CPCM_{10}$ was selected for thermal cycling due to its superior heat transfer properties and leakage resistance. A 2 g $CPCM_{10}$ sample was placed in a crucible for cycle testing. The thermal cycling procedure involved heating the samples to a maximum temperature of 85°C (charging phase) and cooling them to 35°C (discharging phase) to cover the entire phase change range of the PCM. This test was performed for 300 thermal cycles to simulate large operational conditions, and it demonstrated the composite has the capability to keep consistent thermal properties.

After the thermal cycling, the samples underwent meticulous examination to ascertain any potential chemical and thermal alterations. This included visual examination, chemical and thermal stability, and heat storage capability as shown in Figure 11. The visual inspection after the thermal cycles revealed that both the base PCM and the $CPCM_{10}$ composite maintained a homogeneous structure as shown in Figure 11a.

The FTIR spectra of the base PCM and $CPCM_{10}$ after thermal cycling revealed that the primary peaks were observed at 2921, 2851, 1741, 1465, 1166, and 720 as illustrated in Figure 11b. The recorded peaks exhibit a resemblance to those obtained prior to the thermal cycling test. The consistency of these spectral peaks suggests that no significant chemical interactions happened after the thermal cycling. Additionally, Figure 11c illustrates the phase change temperatures along with the latent heat curves following the thermal cycles. The data revealed that both PCM and $CPCM_{10}$ exhibited minimal variations in melting and freezing points, suggesting stability in thermal properties. This minor shift in phase transition temperatures is usually due to minor physical rearrangements in the PCM matrix during repeated thermal cycling. The DSC study was done to determine the retention of latent heat after the thermal cycles. Latent heat capacity was reduced slightly to 104.98 J/g for $CPCM_{10}$ post-cycling, which was associated with the physical stability of EG's porous structure and the ability to hold the PCM in its matrix. Additionally, the minor aggregation of EG/h-BN fillers during cycling may reduce effective energy storage sites, further contributing to the decline [34].

The PCMs exhibited a tendency to degrade when exposed to ongoing cycles of charging and discharging under fluctuating temperature conditions. This may be attributed to the fact that the PCMs absorbed moisture content and contaminants from external ambient conditions [64]. It is anticipated that the PCM would exhibit peculiar behavior when subjected to DSC testing because of the presence of these ambient circumstances and the increased temperature. It has been noticed that the phase transition temperature of the PCM composite shows little variation because of improper crystallization occurring during the phase shift. The phase change temperature of $CPCM_{10}$ composite changed to 64.3°C, while for the base PCM it shifted to 66.1°C. Changes occur in the crystal structure of the sample as well as changes in the thermophysical parameters of the sample when the melting process is complete, and the phase transition occurs from solid to liquid [65]. The thermal decomposition curve of PCM-BW and $CPCM_{10}$ composite after thermal cycling is depicted in Figure 11d. Thermal cycling causes an increase in the breakdown temperature of both the PCM and the composite. The frequent use of PCM causes this phenomenon to be noticeable, as seen in Figure 11. If the PCM composites maintain their decomposition temperature after the thermal cycling test, it indicates the PCM can safely withstand further charging and discharging cycles.

It is worth mentioning the limitation of current thermal reliability testing that although the composites exhibited excellent thermal stability and phase transition consistency, their long-term durability under real environments such as changing humidity and mechanical strain has not been taken into account. The thermal cycles were carried out at predefined temperature conditions (35°C to 85°C) but humidity was not monitored or controlled. Furthermore, the samples were not mechanically loaded or stressed during cycling.

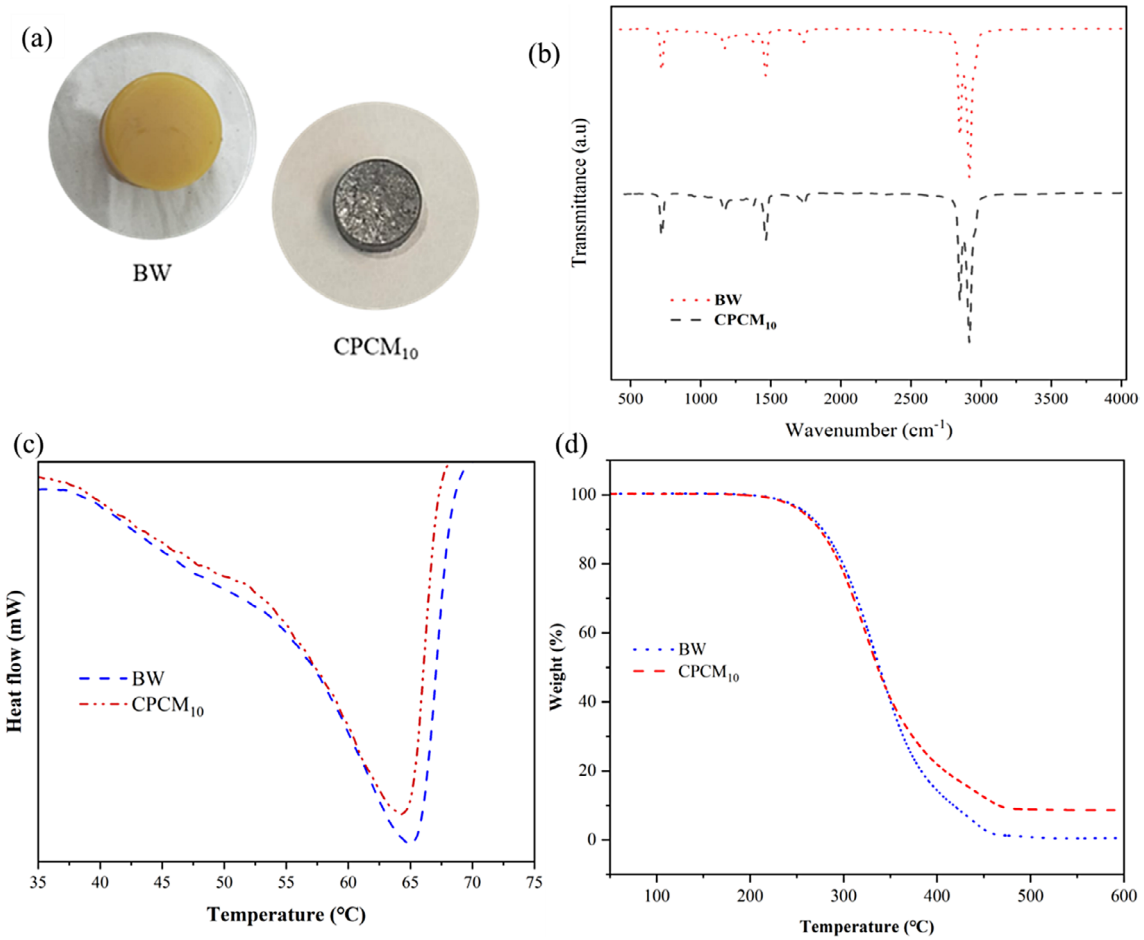

FIGURE 11 | Analysis of thermo-physical behavior of PCM and composites following 300 thermal cycles: (a) digital image of PCM and composite, (b) FTIR analysis, (c) latent heat, (d) thermal decomposition.

3.9 | Thermal to Thermal Conversion

This section employs thermal imaging techniques to investigate the heating and cooling performance of base PCM and CPCM. Samples of base PCM and $CPCM_{10}$ were subjected to heating and cooling cycles on a hot plate, with each cycle extending over a duration of 180 s. During the heating process, temperature measurements were meticulously recorded at regular intervals, with each measurement taken after a duration of 60 s. Furthermore, thermal images have been captured using a digital thermal camera to observe the distribution of temperatures throughout the samples. In a similar manner, data regarding the temperature of the samples as they cooled was also taken over a duration of 180 s following their removal from the heated plate. Immediately following the application of heat, it was observed that the $CPCM_{10}$ demonstrated a rapid temperature rise relative to the base PCM. The temperature of the base PCM attained 56.5°C following the heating duration of 180 s, while the $CPCM_{10}$ was recorded at 60.8°C. The image labeled as $t = 0$ s corresponds to the beginning of Cycle 3, not the initial cycle. As noted, the observed temperature variation at this point is due to residual heat from previous cycles, resulting in a non-uniform initial temperature distribution. The enhanced thermal conductivity and heat transmission capabilities attributed to the additives (h-BN/EG) particles likely account for the accelerated rate of heat transfer. The findings were validated by thermal images captured during the testing process. The application of the additive seems to lead to an improvement in heat transmission efficiency, as evidenced by the increased uniformity in temperature distribution. Both the base PCM and the $CPCM_{10}$ samples demonstrated a progressive decline in temperature throughout the cooling process. Conversely, upon concluding the cooling phase, it was observed that the $CPCM_{10}$ exhibited a temperature that was marginally lower than that of the base PCM. Following the cooling interval of 180 s, the temperature of the base PCM registered precisely at 29°C, whereas the $CPCM_{10}$ exhibited a temperature of 27.4°C, as illustrated in Figure 12. The results of the experiments indicate that $CPCM_{10}$ exhibits superior thermal to thermal conversion performance compared to the base PCM. The $CPCM_{10}$ demonstrates a marked superiority over the PCM, particularly in its capacity for rapid heating and efficient heat dissipation. The integration of h-BN/EG additives into the phase change material presents a substantial opportunity to enhance the efficiency and efficacy of thermal energy storage systems across diverse applications. These applications encompass the thermal regulation of batteries, the insulation of structures, and the storage of renewable energy sources.

4 | Conclusion

This study presents a shape-stabilized composite composed of bio-based beeswax phase change materials (PCMs). It exhibits

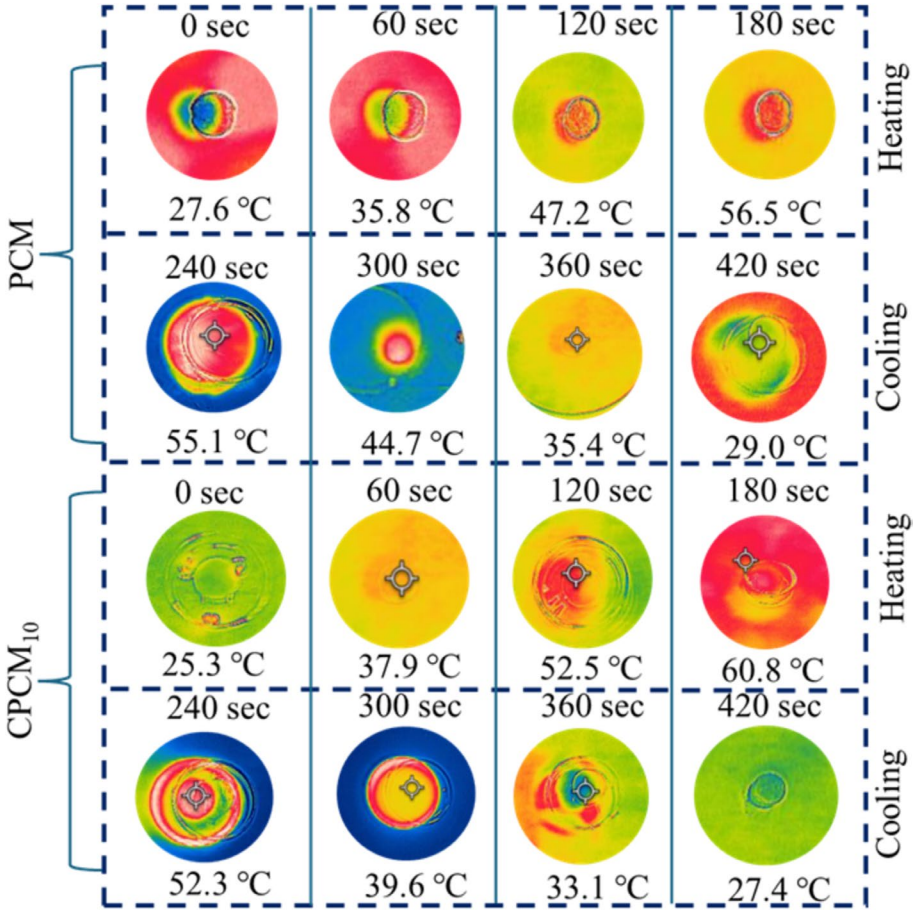

FIGURE 12 | Heat transfer images of PCM and $CPCM_{10}$, illustrating temperature distribution at the beginning of the 3rd cycle.

comparable characteristics and can serve as a viable alternative to commercial options, thus providing a sustainability aspect within PCMs. The research examines the synergistic role of hexagonal boron nitride (h-BN) and EG in enhancing the thermophysical properties of beeswax (BW). The results highlight that the addition of 3% h-BN alongside 10% EG to the base PCM-BW markedly enhanced the thermal conductivity to 1.03 W/m·K, which is a 312% enhancement. Additionally, the $CPCM_{10}$ composite demonstrated anti-leakage characteristics, with only a 12% reduction in latent heat. Moreover, the synthesized PCM composite led to a decrease in optical transmissibility of 68.5%. The composite's reliability was assessed over 300 thermal cycles, demonstrating consistent thermophysical performance. Furthermore, the enhanced composite ($CPCM_{10}$) demonstrated an improvement in thermal-to-thermal conversion of 4.3°C following 180 s of heating, and it enabled a more rapid cooling process with a reduction of 1.6°C after the next 180 s of the cooling phase in comparison to the base PCM. The enhanced thermal conductivity and stable latent heat storage capacity can quickly charge and discharge the thermal energy, making it suitable for thermal regulation in buildings. Furthermore, the higher UV–Vis absorbance and the lower transmittance measured in our optical analysis also indicate the potential applications of solar energy harvesting systems. The CPCM can absorb solar radiation efficiently, store it as latent heat, and gradually release it, which is suitable for solar thermal storage panels or passive heating systems. Moreover, the thermal stability and phase uniformity measured under 300 thermal cycles show that the composite can maintain a consistent performance in realistic environmental conditions. Finally, the good leakage resistance and form stability allow it to be used as an advanced thermal insulator in electronic cooling, cold-chain packaging, and automotive components.

Acknowledgments

The authors acknowledge the support provided by Sunway University for access to research facilities and resources that enabled the completion of this experimental work.

Conflicts of Interest

The authors declare no conflicts of interest.

Data Availability Statement

The data that support the findings of this study are available from the corresponding author upon reasonable request.

References

1. M. A. Gerkman and G. G. D. Han, "Toward Controlled Thermal Energy Storage and Release in Organic Phase Change Materials," *Joule* 4 (2020): 1621–1625.

2. P. Albertus, J. S. Manser, and S. Litzelman, "Long-Duration Electricity Storage Applications, Economics, and Technologies," *Joule* 4 (2020): 21–32.

3. S. Koohi-Fayegh and M. A. Rosen, "A Review of Energy Storage Types, Applications and Recent Developments," *Journal of Energy Storage* 27 (2020): 101047.

4. T. Yang, W. P. King, and N. Miljkovic, "Phase Change Material-Based Thermal Energy Storage," *Cell Reports Physical Science* 2 (2021): 100540.

5. M. A. Rahman, R. Zairov, N. Akylbekov, R. Zhapparbergenov, and S. M. M. Hasnain, "Pioneering Heat Transfer Enhancements in Latent Thermal Energy Storage: Passive and Active Strategies Unveiled," *Heliyon* 10 (2024): e37981.

6. R. Chaturvedi, A. Islam, and K. Sharma, "A Review on the Applications of PCM in Thermal Storage of Solar Energy," *Materials Today: Proceedings* 43 (2021): 293–297.

7. S. Dora, F. Kuznik, and K. M. Mini, "A Novel PCM-Based Foam Concrete for Heat Transfer in Buildings -Experimental Developments and Simulation Modelling," *Journal of Energy Storage* 105 (2025): 114625.

8. S. Kim, R. A. Stavins, V. S. Garimella, et al., "Cooling High Power Electronics Using Dynamic Phase Change Material," *International Journal of Heat and Mass Transfer* 237 (2025): 126433.

9. A. P. Singh, S. Tiwari, and H. Sinhmar, "A Novel Photovoltaic Thermal and Thermoelectric Converter Air Collector Integrated With Solar Dryer Having Thermal Energy Storage—An Experimental Approach," *Journal of Energy Storage* 108 (2025): 115115.

10. J. Bao, H. Tu, J. Li, et al., "Applications of Phase Change Materials in Smart Drug Delivery for Cancer Treatment," *Frontiers in Bioengineering and Biotechnology* 10 (2022): 991005.

11. M. Subramanian, A. T. Hoang, B. Kalidasan, et al., "A Technical Review on Composite Phase Change Material Based Secondary Assisted Battery Thermal Management System for Electric Vehicles," *Journal of Cleaner Production* 322 (2021): 129079.

12. K. Yang, X. Zhang, M. Venkataraman, J. Wiener, and J. Militký, "Phase Change Materials in Textiles for Thermal Regulation," *Advanced Structured Materials* 201 (2023): 27–47.

13. A. A. M. Omara, "Phase Change Materials for Waste Heat Recovery in Internal Combustion Engines: A Review," *Journal of Energy Storage* 44 (2021): 103421.

14. K. Balasubramanian, A. Kumar Pandey, R. Abolhassani, H.-G. Rubahn, S. Rahman, and Y. Kumar Mishra, "Tetrapods Based Engineering of Organic Phase Change Material for Thermal Energy Storage," *Chemical Engineering Journal* 462 (2023): 141984.

15. A.-S. Yang, T.-Y. Cai, L. Su, et al., "Review on Organic Phase Change Materials for Sustainable Energy Storage," *Sustainable Energy & Fuels* 6 (2022): 5045–5071.

16. R. Aridi and A. Yehya, "Review on the Sustainability of Phase-Change Materials Used in Buildings," *Energy Conversion and Management: X* 15 (2022): 100237.

17. U.S. Energy Information Administration (EIA), "Anon Oil and the Environment."

18. F. L. Rashid, M. A. Al-Obaidi, N. S. Dhaidan, et al., "Bio-Based Phase Change Materials for Thermal Energy Storage and Release: A Review," *Journal of Energy Storage* 73 (2023): 109219.

19. R. Mori, "Replacing All Petroleum-Based Chemical Products With Natural Biomass-Based Chemical Products: A Tutorial Review," *RSC Sustainability* 1 (2023): 179–212.

20. "Anon A Systematic Review on Bio-Based Phase Change Materials."

21. D. K. Mishra, S. Bhowmik, and K. M. Pandey, "Development and Assessment of Beeswax/Expanded Graphite Composite Phase Change Material for Thermal Energy Storage," *Arabian Journal for Science and Engineering* 47 (2022): 8985–9004.

22. S. Bogdanov, "Beeswax: Production, Properties Composition and Control BEES PRODUCE WAX," 2009.

23. G. Gupta and K. Anjali, "Environmentally Friendly Beeswax: Properties, Composition, Adulteration, and Its Therapeutic Benefits," *IOP Conference Series: Earth and Environmental Science* 1110 (2023): 012041.

24. M. Ghalambaz and J. Zhang, "Conjugate Solid-Liquid Phase Change Heat Transfer in Heatsink Filled With Phase Change Material-Metal Foam," *International Journal of Heat and Mass Transfer* 146 (2020): 118832.

25. Z. Zhang, Y. He, H. Ma, X. Liu, Y. Zhou, and Y. Yang, "Light/Electro-Thermal Conversion of Carbonized Sweet Potato 3D Grid-Supported PEG Shape-Stable Phase Change Materials for Thermal Management Applications," *Chemical Engineering Research and Design* 210 (2024): 130–139.

26. F. Liu, J. Wang, F. Wang, et al., "Battery Thermal Safety Management With Form-Stable and Flame-Retardant Phase Change Materials," *International Journal of Heat and Mass Transfer* 218 (2024): 124764.

27. Z. Arman, P. Bora, D. Das, and M. M. Phukan, "Green Form-Stable Biocomposite of Biochar From Tea Industry Waste and Organic Phase Change Material," *Journal of Energy Storage* 101 (2024): 113815.

28. J. Deng, X. Li, G. Zhang, et al., "Flexible Composite Phase-Change Material With Shape Recovery and Antileakage Properties for Battery Thermal Management," *ACS Applied Energy Materials* 4 (2021): 13890–13902.

29. A. Sarı, M. Nas, B. Yeşilata, et al., "A Novel Cement Mortar Comprising Natural Zeolite/Dodecyl Alcohol Shape Stable Composite Phase Change Material for Energy Effective Buildings," *Journal of Energy Storage* 87 (2024): 111266.

30. R. Shen, P. Lian, Y. Cao, Y. Chen, L. Zhang, and X. Sheng, "All Lignin-Based Sponge Encapsulated Phase Change Composites With Enhanced Solar-Thermal Conversion Capability and Satisfactory Shape Stability for Thermal Energy Storage," *Journal of Energy Storage* 54 (2022): 105338.

31. X. Cao, C. Li, G. He, Y. Tong, and Z. Yang, "Composite Phase Change Materials of Ultra-High Molecular Weight Polyethylene/Paraffin Wax/Carbon Nanotubes With High Performance and Excellent Shape Stability for Energy Storage," *Journal of Energy Storage* 44 (2021): 103460.

32. X. Xiao, P. Zhang, and M. Li, "Preparation and Thermal Characterization of Paraffin/Metal Foam Composite Phase Change Material," *Applied Energy* 112 (2013): 1357–1366.

33. A. Fethi, L. Mohamed, K. Mustapha, B. Ameurtarek, and B. N. Sassi, "Investigation of a Graphite/Paraffin Phase Change Composite," *International Journal of Thermal Sciences* 88 (2015): 128–135.

34. Y. A. Bhutto, A. K. Pandey, A. Islam, R. K. Rajamony, and R. Saidur, "Lauric Acid Based Form-Stable Phase Change Material for Effective Electronic Thermal Management and Energy Storage Application," *Materials Today Sustainability* 28 (2024): 100931.

35. F. Tarannum, S. Danayat, A. Nayal, R. Muthaiah, R. S. Annam, and J. Garg, "Thermally Expanded Graphite Polyetherimide Composite With Superior Electrical and Thermal Conductivity," *Materials Chemistry and Physics* 298 (2023): 127404.

36. C.-F. Wang, P.-R. Hung, C.-L. Wu, et al., "Synthesis and Thermal Conductivity of Expanded Graphite (EG)/polymer Composites," in *2018 International Conference on Electronics Packaging and iMAPS All Asia Conference (ICEP-IAAC)* (IEEE, 2018), 572–573.

37. P. K. S. Rathore and S. k. Shukla, "Improvement in Thermal Properties of PCM/Expanded Vermiculite/Expanded Graphite Shape Stabilized Composite PCM for Building Energy Applications," *Renewable Energy* 176 (2021): 295–304.

38. A. Islam, A. K. Pandey, R. Saidur, B. Aljafari, and V. V. Tyagi, "Advancements in Foam-Based Phase Change Materials: Unveiling

Leakage Control, Enhanced Thermal Conductivity, and Promising Applications," *Journal of Energy Storage* 74 (2023): 109380.

39. A. Dinker, M. Agarwal, and G. D. Agarwal, "Experimental Study on Thermal Performance of Beeswax as Thermal Storage Material," *Materials Today Proceedings* 4 (2017): 10529–10533.

40. S. N. Kallaev, A. G. Bakmaev, A. A. Babaev, A. R. Bilalov, Z. M. Omarov, and E. I. Terukov, "Thermophysical Properties of Thermally Expanded Graphite," *High Temperature* 60 (2022): 15–18.

41. K. A. Bello, M. A. Maleque, and Z. Ahmad, "Synthesis and Characterization of Ni–P Coated Hexagonal Boron Nitride by Electroless Nickel Deposition," *Surface Engineering and Applied Electrochemistry* 51 (2015): 523–529.

42. "Anon FTIR Analysis | RTI Laboratories."

43. S. Gunasekaran, R. K. Natarajan, and A. Kala, "FTIR Spectra and Mechanical Strength Analysis of Some Selected Rubber Derivatives," *Spectrochimica Acta. Part A, Molecular and Biomolecular Spectroscopy* 68 (2007): 323–330.

44. X. Du, S. Wang, Z. Du, X. Cheng, and H. Wang, "Preparation and Characterization of Flame-Retardant Nanoencapsulated Phase Change Materials With Poly(Methylmethacrylate) Shells for Thermal Energy Storage," *Journal of Materials Chemistry A* 6 (2018): 17519–17529.

45. A. Islam, A. K. Pandey, R. Saidur, and V. V. Tyagi, "Shape Stable Composite Phase Change Material With Improved Thermal Conductivity for Electrical-to-Thermal Energy Conversion and Storage," *Materials Today Sustainability* 25 (2024): 100678.

46. W. Wu, J. Liu, M. Liu, et al., "An Innovative Battery Thermal Management With Thermally Induced Flexible Phase Change Material," *Energy Conversion and Management* 221 (2020): 113145.

47. M. M. Hamed, A. El-Tayeb, I. Moukhtar, A. Z. El Dein, and E. H. Abdelhameed, "A Review on Recent Key Technologies of Lithium-Ion Battery Thermal Management: External Cooling Systems," *Results in Engineering* 16 (2022): 100703.

48. J.-L. Zhang, N. Wu, X.-W. Wu, et al., "High Latent Heat Stearic Acid Impregnated in Expanded Graphite," *Thermochimica Acta* 663 (2018): 118–124.

49. D. Zhou, S. Xiao, and Y. Liu, "The Effect of Expanded Graphite Content on the Thermal Properties of Fatty Acid Composite Materials for Thermal Energy Storage," *Molecules* 29 (2024): 3146.

50. Z. Wang, C. Du, R. Qi, and Y. Wang, "Experimental Study on Thermal Management of Lithium-Ion Battery With Graphite Powder Based Composite Phase Change Materials Covering the Whole Climatic Range," *Applied Thermal Engineering* 216 (2022): 119072.

51. J. Mei, G. Shi, H. Liu, Z. Wang, and M. Chen, "Investigation on the Optimization Strategy of Phase Change Material Thermal Management System for Lithium-Ion Battery," *Journal of Energy Storage* 55 (2022): 105365.

52. C. Ma, Y. Zhang, S. Hu, X. Liu, and S. He, "A Copper Nanoparticle Enhanced Phase Change Material With High Thermal Conductivity and Latent Heat for Battery Thermal Management," *Journal of Loss Prevention in the Process Industries* 78 (2022): 104814.

53. Y. Zhang, J. Huang, M. Cao, Z. Liu, and Q. Chen, "A Novel Flexible Phase Change Material With Well Thermal and Mechanical Properties for Lithium Batteries Application," *Journal of Energy Storage* 44 (2021): 103433.

54. X. Lin, X. Zhang, L. Liu, J. Liang, and W. Liu, "Polymer/Expanded Graphite-Based Flexible Phase Change Material With High Thermal Conductivity for Battery Thermal Management," *Journal of Cleaner Production* 331 (2022): 130014.

55. N. Zheng, C. Zhang, R. Fan, and Z. Sun, "Melamine Foam-Based Shape-Stable Phase Change Composites Enhanced by Aluminum Nitride for Thermal Management of Lithium-Ion Batteries," *Journal of Energy Storage* 52 (2022): 105052.

56. W. Wu, S. Wang, W. Wu, K. Chen, S. Hong, and Y. Lai, "A Critical Review of Battery Thermal Performance and Liquid Based Battery Thermal Management," *Energy Conversion and Management* 182 (2019): 262–281.

57. P. K. S. Rathore and S. K. Shukla, "Potential of Macroencapsulated PCM for Thermal Energy Storage in Buildings: A Comprehensive Review," *Construction and Building Materials* 225 (2019): 723–744.

58. A. Chandra and A. Chandra, "Ion Conduction Mechanism of Nanoparticle-Based Polymer Composites," in *Nanoparticle-Based Polymer Composites* (Elsevier, 2022), 277–306.

59. Y. Shu, J. He, D. Xu, et al., "Mechanical and Thermal Behavior of PBAT Matrix Composites Filled With Lignin," *Journal of Polymer Research* 32 (2025): 56.

60. A. Yousefi, W. Tang, M. Khavarian, and C. Fang, "Development of Novel Form-Stable Phase Change Material (PCM) Composite Using Recycled Expanded Glass for Thermal Energy Storage in Cementitious Composite," *Renewable Energy* 175 (2021): 14–28.

61. A. Balaji, R. Saravanan, R. Purushothaman, S. Vijayaraj, and P. Balasubramanian, "Investigation of Thermal Energy Storage (TES) With Lotus Stem Biocomposite Block Using PCM," *Cleaner Engineering and Technology* 4 (2021): 100146.

62. A. Yadav, A. K. Pandey, M. Samykano, T. Kareri, and V. V. Tyagi, "Wheat Husk Derived Microparticle Infused Organic Phase Change Material for Efficient Heat Transfer and Sustainable Thermal Energy Storage," *Journal of Energy Storage* 86 (2024): 111204.

63. H. Li, H. Jia, K. Zhong, and Z. Zhai (John), "Analysis of Factors Influencing Actual Absorption of Solar Energy by Building Walls," *Energy* 215 (2021): 118988.

64. A. Anand, A. Shukla, A. Kumar, D. Buddhi, and A. Sharma, "Cycle Test Stability and Corrosion Evaluation of Phase Change Materials Used in Thermal Energy Storage Systems," *Journal of Energy Storage* 39 (2021): 102664.

65. Q. Zhang, T. C. Le, S. Zhao, et al., "Advancements in Nanomaterial Dispersion and Stability and Thermophysical Properties of Nano-Enhanced Phase Change Materials for Biomedical Applications," *Nanomaterials (Basel)* 14 (2024): 1126.